Available online at www.sciencedirect.com
ScienceDirect
Trans. Nonferrous Met. Soc. China 33(2023) 2287−2302
Transactions of Nonferrous Metals Society of China
www.tnmsc.cn

Microstructure and mechanical properties of Al−Zn−Mg−Cu (7075) alloy tubes prepared via power stagger spinning

Fan-lin ZHENG[1,2], Hong-sheng CHEN[1,2], Wen-xian WANG[3], Hui-liang GAO[1], Yong-kang GAO[1]

1. College of Mechanical and Vehicle Engineering, Taiyuan University of Technology, Taiyuan 030024, China;
2. Shanxi Key Laboratory of Intelligent Underwater Equipment, Taiyuan 030024, China;
3. College of Materials Science and Engineering, Taiyuan University of Technology, Taiyuan 030024, China

Received 2 February 2022; accepted 23 May 2022

Abstract: The tubes of 7075 aluminum alloy were fabricated by power stagger spinning at 400 °C (HS) and room temperature (RTS), and then the microstructure evolution and mechanical properties were investigated. Results show that the grains after spinning are refined prominently, and the tubes after 60% and 70% thickness reduction (HS-60% and HS-70%) are dominated by the deformed structure, while the recrystallized structure is dominant in the tube after 85% thickness reduction at 400 °C (HS-85%). Furthermore, a bimodal grain structure with a weak Cube texture is obtained in the HS-85% sample due to the emergence of the dynamic recrystallization (DRX) and abnormal grain growth. As the thickness reduction increases from 0% to 85% during spinning at 400 °C, the yield strength (YS) and ultimate tensile strength (UTS) increase first and then decrease, while the elongation decreases first and then increases. Compared with that of the HS-85% sample, the UTS and YS of RTS-85% sample are 613.5 and 567.9 MPa, respectively, which are improved by 33.7% and 57.4%, while the elongation is only 7.3%.

Key words: 7075 aluminum alloy; power stagger spinning; microstructure evolution; bimodal grain structure; abnormal grain growth; mechanical properties

1 Introduction

Tube spinning is an advanced and effective plastic deformation process to produce hollow rotary components, which belongs to one of the near net-shape forming technologies [1,2]. In fact, spinning forming technology can be treated as a combination of rotary forming and plastic forming. Combining the advantages of both, it has the preponderance of high material utilization, fast forming, good surface quality, high precision and low consumption [3,4]. Therefore, the spinning technology has been widely used in the aviation, aerospace, weapons and automobile industries [5,6]. 7075 aluminum alloy mainly composed of Al, Zn, Mg and Cu elements, belongs to a kind of super hard aluminum alloy of 7000 series and has the advantages of light weight, high specific strength and specific stiffness, good fracture toughness and excellent molding performance [7−9], which makes the tube made from 7075 aluminum alloy have a great application prospect in the field of lightweight. Therefore, it is necessary to investigate the formability of 7075 alloy tube during spinning for providing technical supports of the plastic processing.

At present, some research has been reported on the spinning forming of 7075 aluminum alloys. ZHANG et al [10] investigated the effects of the process parameters on elongation during hot power backward spinning for 7075 cast aluminium alloy

Corresponding author: Hong-sheng CHEN, Tel: +86-18334704835, E-mail: chenhongsheng@tyut.edu.cn
DOI: 10.1016/S1003-6326(23)66259-4
1003-6326/© 2023 The Nonferrous Metals Society of China. Published by Elsevier Ltd & Science Press

tube combined with the FE analysis. They reported that the elongation of the spun tube increased gradually with the increase of preheating temperature and roller fillets radius, while sharply decreased and then tended to a stable value with the increase of the roller feed rate. ZHANG et al [11] also researched the evolution regularity of temperature field of 7075 alloy tube during spinning. They claimed that the high temperature region was transferred from unformed zone of the tube to the contact area between spinning roller and tube, and in the spinning zone, the temperature of internal surface of the tube was apparently higher than that of the outer face. MOLLADAVOUDI and DJAVANROODI [12] investigated the effects of the thickness reduction on mechanical properties and spinning accuracy of 7075 alloy tubes during flow forming. They claimed that with increment of thickness reduction, the yield strength, ultimate strength, surface hardness, and crystal refining increased, while it had adverse effects on diameter growth, geometrical accuracy, surface roughness, and elongation of spun tube. It is well known that the microstructure essentially determines the mechanical properties of materials [13]. However, much research has been reported on the microstructure evolution of 7075 alloy tubes during spinning process. Therefore, it is necessary to systematically study the microstructure evolution and further investigate the variation of mechanical properties during spinning, which is of great research significance.

In this work, the 7075 aluminum alloy tubes were fabricated by tube spinning technology, i.e., power stagger spinning. The evolution of microstructure and the mechanical properties of 7075 aluminium alloy tubes during spinning were revealed, and the strengthening mechanisms were analyzed. This work provides a theoretical basis for the preparation of thin-wall 7075 aluminum alloy tube with controllable structure and performance.

2 Experimental

2.1 Materials and spinning process

In this study, the hot extruded bars of 7075 aluminum alloy with a diameter of 44 mm were used as the as-received material. The chemical composition of 7075 alloy is shown in Table 1. The microstructure of the as-received material is presented in Fig. 1. As shown, the as-received material has a typical extruded structure and is composed of fine equiaxed grains and coarse elongated grains, and the average grain size is 25.4 μm.

The hot extruded bars were machined into tube billets with one end closed by subsequent machine work and the size is shown in Fig. 2(a). Then, the tube billets were processed by three-roller power stagger forward spinning at 400 °C and room temperature. The samples were spun with various thickness reductions of 60%, 70% and 85% at 400 °C (hereafter labeled HS-60%, HS-70% and HS-85%, respectively), and the sample was spun at room temperature with 85% thickness reduction (hereafter labeled RTS-85%). The spinning assembly diagram of the fabricated 7075 alloy tubes is shown in Fig. 2(b). The rotating speed of the mandrel was 160 r/min and the feed rate of the rollers was 1 mm/r. In addition, before the spinning at 400 °C, the tube blanks were heated at 400 °C for 10 min, and the preheating temperature of the mandrel was 200 °C. The specific process parameters during spinning are presented in Table 2.

Table 1 Chemical composition of 7075 alloy (wt.%)

Cu	Mg	Zn	Fe	Si	Mn	Cr	Al
2.0	2.5	5.6	0.5	0.4	0.3	0.2	Rest

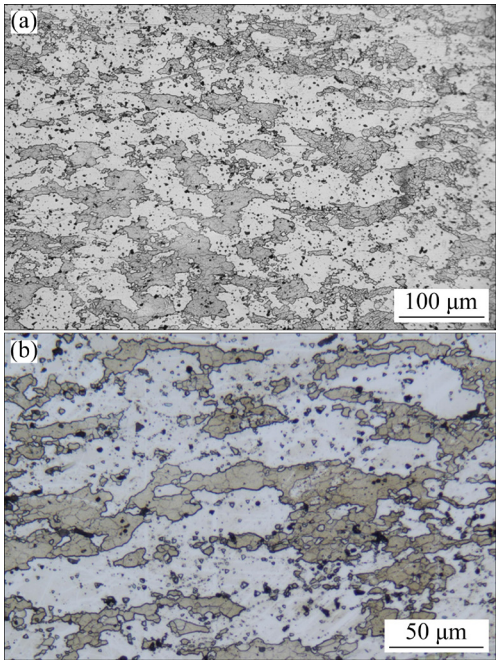

Fig. 1 Microstructure of original extruded 7075 alloy

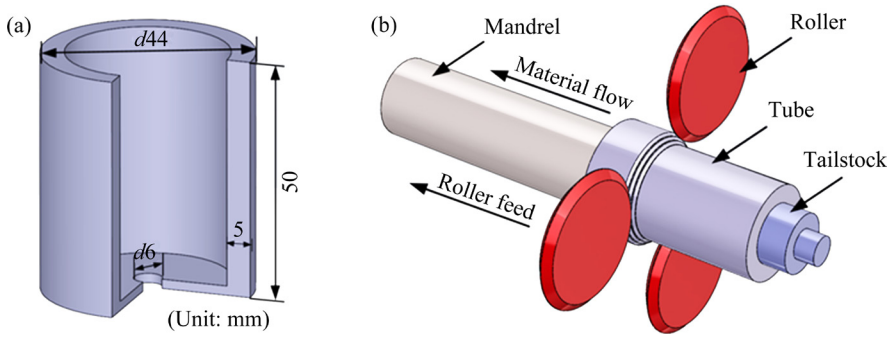

Fig. 2 Machined tube billet size (a) and spinning assembly diagram of fabricated 7075 alloy tubes (b)

Table 2 Process parameters during spinning

Sample	Total thickness reduction/%	Temperature/ °C	Total pass	Initial wall thickness/mm	Final wall thickness/mm
HS-60%	60	400	One pass	5	2
HS-70%	70	400	Two pass	5	1.5
HS-85%	85	400	Three pass	5	0.75
RTS-85%	85	Room temperature	Two pass	5	0.75

2.2 Microstructure and mechanical property analysis

The RD, AD and TD stand for radial/thickness direction, axial direction and tangential direction, respectively. The metallographic specimen of the as-received tube was cut parallel to the TD−RD plane (cross section) of the tube. The specimen was ground, mechanically polished and etched with a Keller solution for 10−20 s, and then the microstructure was characterized by optical microscope (OM). The detailed microstructure, grain orientation and texture evolution on AD−RD plane (longitudinal section) during spinning were investigated by scanning electron microscopy (SEM) equipped with an electron backscatter diffraction (EBSD, Oxford Instruments) system and transmission electron microscopy (TEM). The test planes of the EBSD specimens and TEM specimens were parallel to the AD−RD plane of the 7075 alloy tubes, as shown in Fig. 3. The EBSD specimens were electrochemical polished with a mixed solution of 10% $HClO_4$ and 90% ethanol for 35 s. The voltage and electric current in electrochemical polishing were 20 V and 0.3 A, respectively. The TEM samples were firstly mechanically ground to about 50 μm in thickness, and then perforated by ion milling under the angle of 3° with an ion accelerating voltage of 3 kV. The specimens for tensile test were cut along the AD and tested at room temperature using a displacement rate of 0.2 mm/min on a universal testing machine. The location and size of tensile specimens are shown in Fig. 3. After the tensile test, the fracture surfaces of the specimens were investigated by SEM.

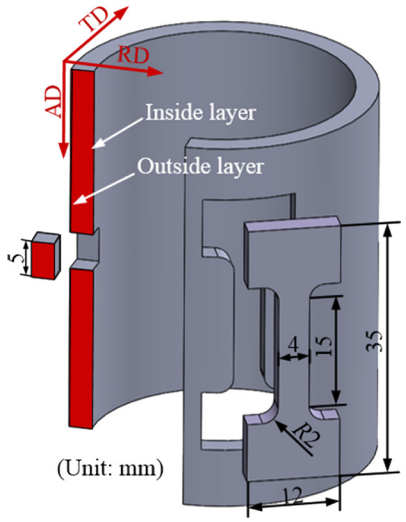

Fig. 3 Sampling location of EBSD and TEM samples, and sampling location and size of tensile specimen

3 Results and discussion

3.1 Microstructure evolution of 7075 alloy tubes during spinning at 400 °C

Figure 4 shows the EBSD measurements of the tubes in the AD−RD plane with different thickness

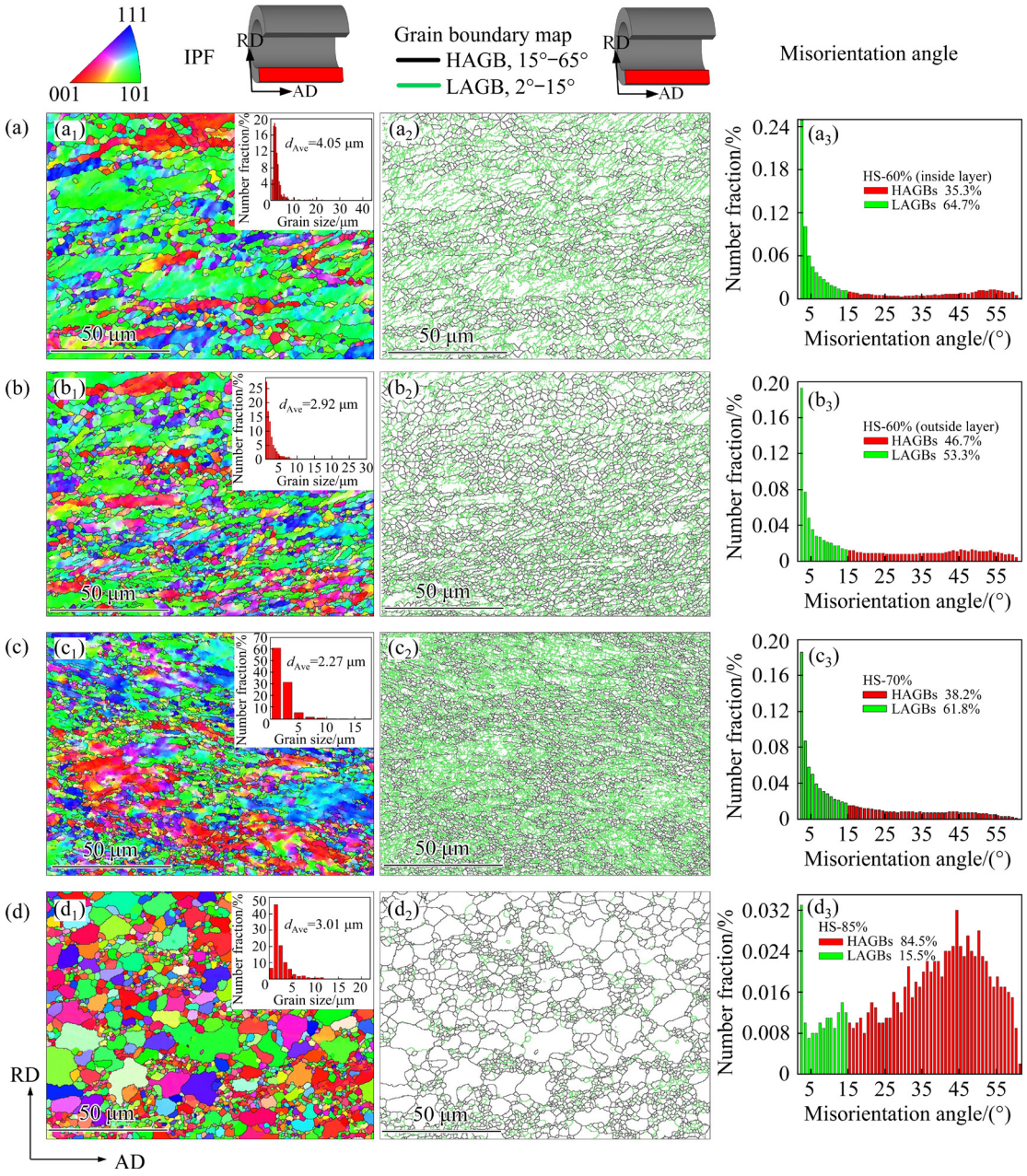

Fig. 4 Inverse pole figure (IPF) maps (a_1, b_1, c_1, d_1), grain boundary maps (a_2, b_2, c_2, d_2), and misorientation angle frequency histograms (a_3, b_3, c_3, d_3) of 7075 alloy with different reductions at 400 °C: (a) HS-60% (inside); (b) HS-60% (outside); (c) HS-70%; (d) HS-85%

reductions after spinning at 400 °C. Different color contrasts in the IPF mapped in Fig. 4 correspond to different grain orientations. As presented in Fig. 4(a_1), the grains on the inside layer of tube after 60% thickness reduction are significantly elongated along the AD and the width/height ratio of the grains increases, and the average grains size (d_{Ave}) is 4.05 μm, which is prominently refined compared with the as-received grains due to the severe plastic deformation. However, as shown in Fig. 4(b_1), compared with that on the inside layer, the grains on the outside layer are distinctly more fragmentary and finer, and the d_{Ave} is 2.92 μm. This suggests the uneven deformation along the RD of the tube after 60% thickness reduction due to the fact that the shear strain does not evenly run through the full wall thickness. With further increasing the thickness reduction to 70%, as expected, the grains are finer and the d_{Ave} is 2.27 μm, as indicated in Fig. 4(c_1). Nevertheless, with increasing the thickness reduction to 85%, a bimodal grain structure with the d_{Ave} of 3.01 μm occurs in the microstructure, and

the maximum grain size approaches 21 μm and the size of fine grains is mainly concentrated at about 1.5 μm. YU et al [14] associated a d_{max}/d_{Ave} of more than 3 with the appearance of abnormal grain growth, where d_{max} is the average size of the largest 2% grains and d_{Ave} is the average grain size. Based on the microstructure illustrated in Fig. 4(d_1), the ratio is about 5.2 for the HS-85% sample. The result indicates that an abnormal grain growth may take place during the three-pass spinning with 85% thickness reduction at 400 °C, resulting in the increase of the d_{Ave}.

The grain boundary maps in Fig. 4 show that the black and green lines indicate the location of high angle grain boundaries (HAGBs, 15°−65°) and low angle grain boundaries (LAGBs, 2°−15°), respectively. As seen from Figs. 4(a_2, b_2) and (a_3, b_3), the LAGBs mainly distribute in the interior of the coarse grains after 60% thickness reduction, and the HAGBs with the number fraction of 46.7% on the outside layer are more than 35.3% that on the inside layer, which may be attributed to the fact that the grains on the outside layer fragment into many smaller grains due to the greater plastic deformation. As shown in Fig. 4(c_3), compared with that of the HS-60%(outside) sample, the number fraction of LAGBs of HS-70% sample increases slightly, which may be due to the more accumulation of dislocation and formation of subgrains [15]. It is noteworthy that when the thickness reduction is up to 85%, the LAGBs mainly distribute in the fine grain interior, and the fraction of LAGBs decreases to 15.5% and the fraction of HAGBs significantly increases to 84.5%, as presented in Figs. 4(d_2) and (d_3). This may be considered to be concerned with the emergence of the dynamic recovery (DRV) and dynamic recrystallization (DRX) during spinning at 400 °C.

Figure 5 shows the pole figures of 7075 alloy tubes at different thickness reductions at 400 °C, and the corresponding texture component is marked in the {111} pole figure according to Refs. [16,17]. As shown in Figs. 5(a) and (b), the maximum texture intensity of the HS-60% sample on the inside and outside layers are found to be 8.68 and 6.80, respectively, and the HS-60% sample exhibits the strong so-called β-fiber texture components containing the S{123}⟨634⟩ texture and Brass {110}⟨112⟩ texture. As indicated in Fig. 5(c), after 70% thickness reduction, the maximum texture intensity drops to 4.94, and a weak S texture exists in the microstructure. With increasing the thickness reduction to 85%, the maximum texture intensity increases slightly to 5.63, and the deformation texture of S texture and Brass texture almost disappears and is replaced by newly generated Cube {100}⟨010⟩ texture. Furthermore, the direction of the texture on the {100} crystal face is distributed obviously in the *Y*0 direction, as shown in Fig. 5(d).

The recrystallized, substructured and deformed microstructures of the 7075 alloy tubes with different thickness reductions are presented in Fig. 6. The quantitative analysis of deformed, substructured and recrystallized structures is shown in Fig. 7. As shown in Figs. 6(a) and (b), after 60% thickness reduction, the deformed grains are dominant in the microstructure and the fractions on the inside layer and outside layer are 83% and 79%, respectively. This implies the emergence of numerous dislocation multiplication and entanglement, which results in the high fraction of LAGBs and the occurrence of the deformation texture. The similar phenomenon can be observed at HS-70% sample from Fig. 6(c) and the deformed grains account for 90%. Nevertheless, with increasing the thickness reduction to 85%, the deformed grains descend obviously, and the recrystallized grains ascend remarkably accounting for about 74%. This suggests the emergence of a dynamic recrystallization (DRX), which leads to the increase of HAGBs (Fig. 4(d_3)). Moreover, the fine grains are composed of numerous deformed and substructured grains and some recrystallized grains, while the coarse grains mainly consist of the recrystallized grains. This means that different mechanisms in the formation of the fine grains and coarse grains are involved. It is well believed that high deformation temperature can accelerate the DRV and activate the DRX in aluminium alloys [18]. The DRV and DRX occur easily in the aluminium with high stack energy (SE), which can promote the climb and cross slip of dislocations [19,20]. And the large shear strain can increase the stored energy, which provides a higher driving force for the recrystallization and the grain growth [21−23]. Therefore, the main reason to form the fine grains in the sample of HS-85% is due to the combined effect of DRV and DRX, while the formation of the coarse grains can be attributed to

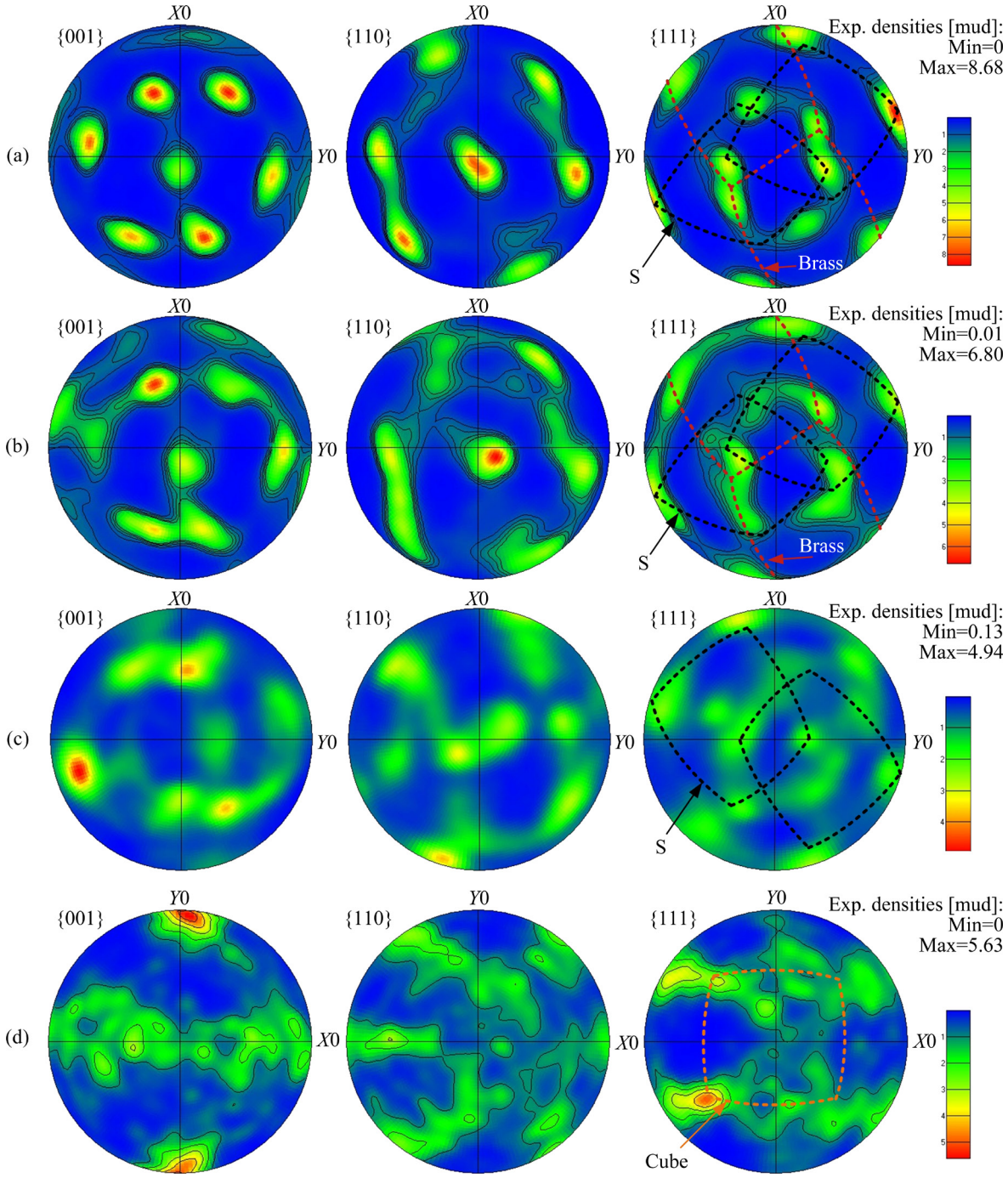

Fig. 5 Poles figures of 7075 alloy tubes with different thickness reductions at 400 °C: (a) HS-60% (inside); (b) HS-60% (outside); (c) HS-70%; (d) HS-85%

the abnormal grain growth of the related grain boundary migration during DRX. LI et al [24] indicated that under the high temperature and high strain, the grain boundaries of some grains may move towards other grains around them, and the merging of grains completes this specific process of grain growth. In this work, the driving force of the formation of coarse grains is the high temperature of 400 °C and the large spinning deformation of 85%. Moreover, the sample of HS-85% undergoes the deformation of three passes at 400 °C. The three passes mean that the heat input of the HS-85% sample is higher than that of other samples due to the longer heating time, which may be another cause for the formation of coarse grains. And the DRX and the abnormal growth of grains are the

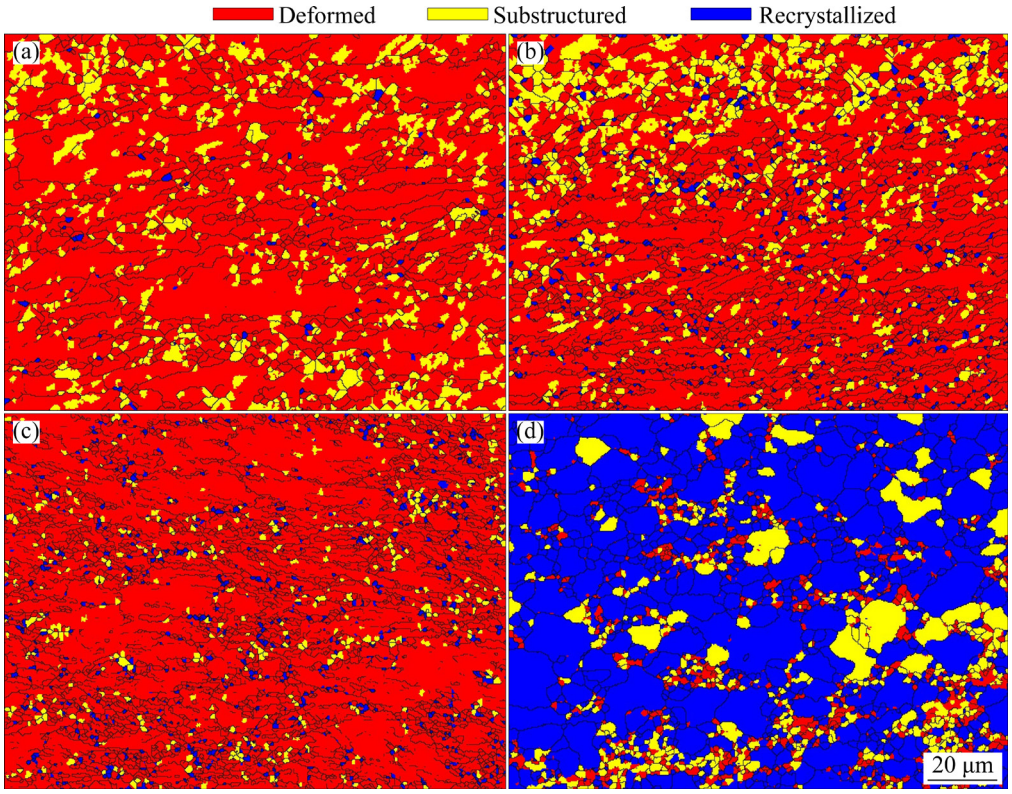

Fig. 6 Recrystallized, substructured and deformed microstructures of 7075 alloy tubes with different thickness reductions: (a) HS-60% (inside); (b) HS-60% (outside); (c) HS-70%; (d) HS-85%

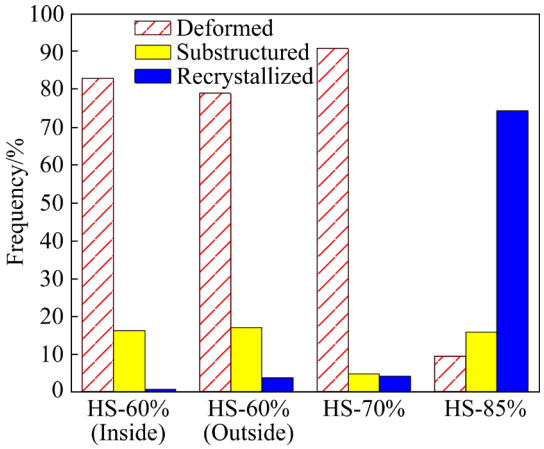

Fig. 7 Recrystallized, substructured and deformed frequency of 7075 alloy tubes with different thickness reductions

main cause of the occurrence of the Cube texture and the drop of the deformation texture components (Fig. 5(d)) [25].

Figure 8 displays the measured kernel average misorientation (KAM) maps of the 7075 alloy tubes under different thickness reductions. The KAM can be used to analyze the local strain distribution [26,27]. And the color scale illustrates the local misorientation degree, which directly represents the internal strain at individual measured points [28]. Meanwhile, local crystal orientations can be measured to study the geometrically necessary dislocations (GND) evolution [29]. At 60% thickness reduction, the sample of HS-60% exhibits an outstanding local stain distribution and the average KAM angles on the inside and outside layers are 1.30 and 1.24, respectively, which suggests the high internal strain energy and dislocation density after 60% thickness reduction, as shown in Figs. 8(a) and (b). Moreover, a noteworthy large KAM angle can be found in the vicinity of the grain boundaries, which may be due to the fact that a large number of dislocations pile up near grain boundaries. With further increasing the thickness reduction to 70%, the average KAM value of HS-70% sample is 1.52, indicating the higher internal strain energy and severer dislocation pile-up. As presented in Fig. 8(d), after 85% thickness reduction, the internal strain energy and dislocation density are obviously lower due to the occurrence of DRX, and the HS-85% sample possesses the lowest average KAM value of 0.55. Furthermore, the local strain is mainly concentrated in the fine grains due to the incomplete DRX.

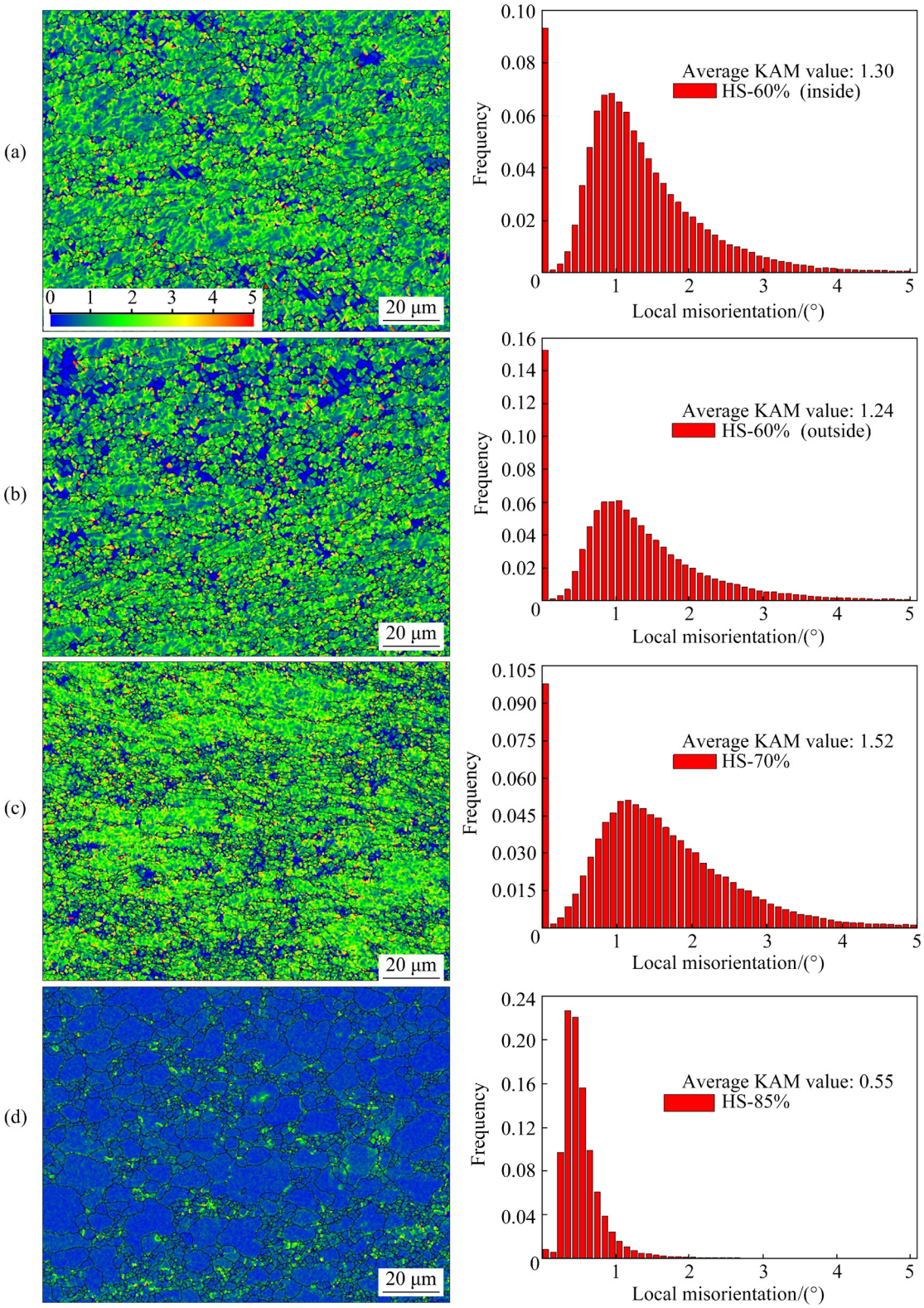

Fig. 8 KAM maps measured in 7075 alloy tube under different passes at 400 °C: (a) HS-60% (inside); (b) HS-60% (outside); (c) HS-70%; (d) HS-85%

The schematic diagram illuminating the mechanism of grain refinement and grain abnormal growth during spinning at 400 °C is presented in Fig. 9. After small spinning deformation, the grains are elongated, and numerous dislocation multiplication occurs inside deformed grains, as shown in Fig. 9(b). As presented in Fig. 9(c), with the increase of the spinning deformation, the

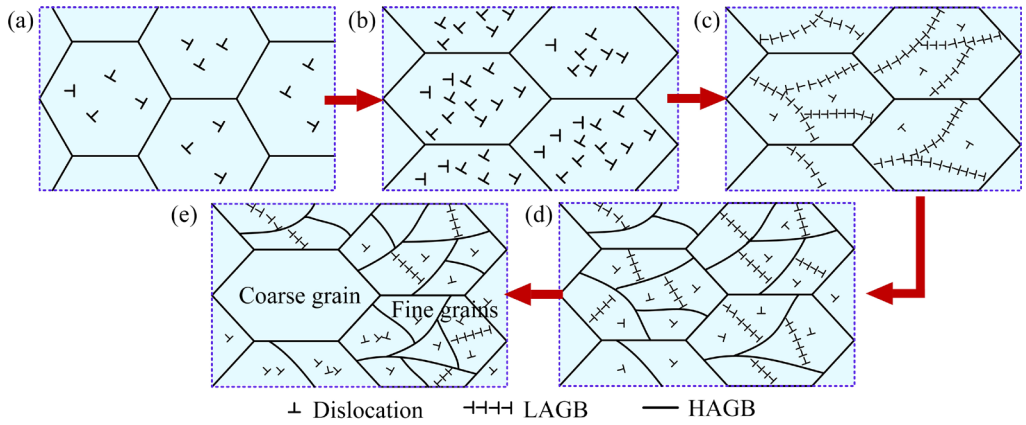

Fig. 9 Schematic diagram of mechanism of grain refinement and grain growth during spinning at 400 °C: (a) Grains before deformation; (b) Increase of dislocations; (c) Formation of LAGBs; (d) Transformation of some of LAGBs to HAGBs and grain refinement; (e) Abnormal grain growth

dislocations can be rearranged into the LAGBs, and subsequently into the dislocation cells in order to minimize the strain energy and form cell boundaries [30,31]. With further increasing the spinning deformation, under the high temperature and high plastic strain, not only more dislocations generate and are absorbed by the LAGBs, but also the dislocation cells start to rotate, so that the misorientation angle between them increases and some of LAGBs transform to HAGBs via constantly consuming the dislocations [32−34], which results in the grain refinement and increase of HAGBs, as illustrated in Fig. 9(d). The LAGBs possess lower energy and mobility, while the grains with HAGBs could grow abnormally due to their higher energy and mobility [35]. As a consequence, the increase of the fraction of HAGBs stimulates the abnormal grain growth, which results in the emergence of a bimodal grain structure, as presented in Fig. 9(e).

3.2 Mechanical properties of 7075 alloy tubes during spinning at 400 °C

Figure 10 displays the mechanical properties of the 7075 aluminum alloy tubes with different thickness reductions, and the corresponding yield strength (YS), ultimate tensile strength (UTS) and elongation are shown in Table 2. As shown, with the increase of thickness reduction, the YS and UTS increase first and then decrease, while the elongation decreases first and then increases. It is well known that the grain refinement can improve both the strength and plasticity of the material,

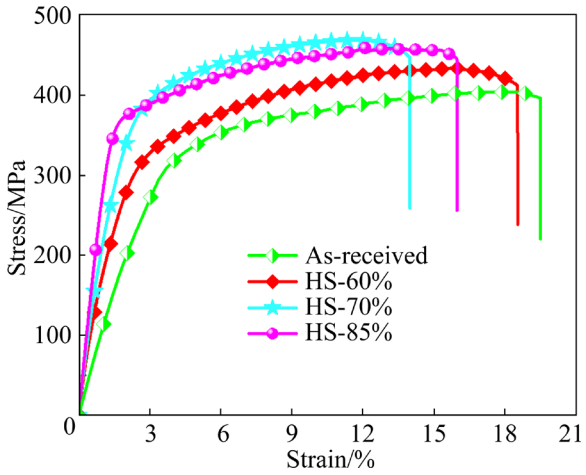

Fig. 10 Tensile stress−strain curves of 7075 aluminum alloy tubes with different thickness reductions

Table 2 Tensile properties of 7075 alloy tubes under different thickness reductions at 400 °C

Sample	YS/MPa	UTS/MPa	Elongation/%
As-received	293.8	403.7	19.6
HS-60%	324.3	433.7	18.5
HS-70%	365.0	468.8	14.0
HS-85%	360.7	458.9	15.9

while the high density dislocation pile-up is conducive to the strength but is detrimental to the ductility. Therefore, as the thickness reduction increases from 0% to 70%, the increase of the YS and UTS and the decrease of elongation of 7075 alloy tube are mainly attributed to the synergistic effect of the grain refinement and work hardening, and the maximum YS of 365.0 MPa and UTS of

468.8 MPa and the minimum elongation of 14.0% are obtained after 70% thickness reduction. Moreover, the strong shear deformation can reduce the pore defect during the plastic deformation and improve the compactness [36]. Hence, after 60% thickness reduction, the slight decrease of the elongation may be closely related to the grain refinement and the improvement of compactness, while the obvious decrease of elongation after 70% thickness reduction is attributed to the severe pile-up of dislocations. The DRV and DRX can cause the reduction of work hardening via promoting the rearrangement and annihilation of dislocations, and the HS-85% sample possesses the high fraction of recrystallized grains. As a consequence, as the spinning deformation increases from 70% to 85%, the decrease of YS and UTS is mainly due to the fact that the effect of the DRX is higher than that of the working hardening. In addition, HE et al [37] illustrated that as the coarse grain domain in the bimodal structure had lower yield stress and larger failure strain, it can resist rapid propagation of the crack to enhance the overall ductility of the alloy. And GUO et al [38] and ZHANG et al [39] illustrated that the bimodal grain structure can cause an increase of formability, and in such a microstructure, with the increase of applied stress, coarse grains deformed first due to the lower yield stress, and fine grains deformed later. Therefore, the increase of elongation of the HS-85% sample is mainly attributed to the formation of bimodal grains and the weakening of work hardening.

Figure 11 presents the fracture morphologies of the 7075 alloy tubes under different thickness reductions. As shown in Figs. 11(c−h), after spinning, the sizes of dimples are obviously smaller, which is mainly attributed to the refinement of grains caused by severe plastic deformation, and numerous small equiaxed dimples on the fracture faces indicate that the main fracture mechanism belongs to the dimple-induced transgranular fracture. In addition, many shear dimples (marked by red arrows) could be found in the local area of Figs. 11(e) and (f), which is attributed to the strong stress concentration due to the high dislocation density after 70% thickness reduction, so the ductility of the HS-70% sample exhibits an obvious decrease. This indicates that in addition to the dimple-induced transgranular fracture, the quasi-cleavage fracture is also the fracture mechanism of the HS-70% sample.

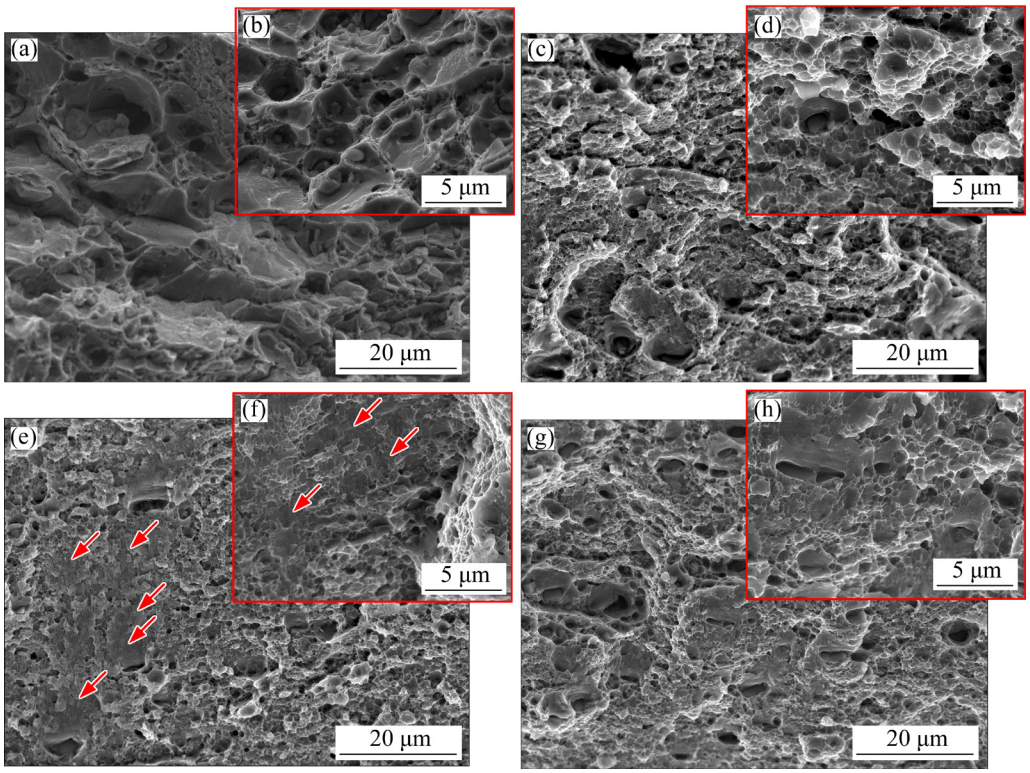

Fig. 11 SEM fracture surfaces of 7075 alloy tubes under different thickness reductions: (a, b) As-received; (c, d) HS-60%; (e, f) HS-70%; (g, h) HS-85%

In order to understand the effect of microstructure on the evolution of mechanical properties and fracture mechanism during spinning at 400 °C in more detail, the further explanations are given below. By 60% spinning deformation, the grain size descends from 25.6 μm to 2.92−4.05 μm (Figs. 4(a_1) and (b_1)). Grain refinement can contribute to the improvement of mechanical properties according to the Hall−Petch effect [40]. Furthermore, the obvious local strain distribution (see Figs. 8(a) and (b)) due to the accumulation of dislocations in HS-60% sample indicates a strong working hardening. As a result, the combined effect of the grain refinement and working hardening improves the YS and UTS of HS-60% sample. However, as the damage of the working hardening to elongation is greater than the contribution of the grain refinement, the elongation of HS-60% sample shows a slight decrease, and the dimples become shallow on the fracture surface and the fracture mechanism is the dimple-induced transgranular fracture. With further spinning to 70%, the grain size (Fig. 4(c_1)) is slightly reduced compared to the HS-60% sample, while the working hardening is more significant (Fig. 8(c)). This leads to the fact that the elongation descends and the strength ascends obviously, and the maximum YS and UTS and the minimum elongation are obtained during spinning at 400 °C. And the fracture mechanism is a mixture of the dimple-induced transgranular fracture and quasi-cleavage fracture (Figs. 11(e) and (f)). As the thickness reduction increases from 70% to 85%, the dislocation density (Fig. 8(d)) decreases and the mean grain size (Fig. 4(d_1)) increases slightly from 2.27 to 3.01 μm due to the occurrence of the dynamic recrystallization (DRX) and the abnormal grain growth, which results in the decrease of the YS and UTS and the increase of elongation of HS-85% sample. In addition, the bimodal grain structure in the HS-85% also contributes to the improvement of elongation due to the fact that the coarse grain can resist rapid propagation of the crack. Hence, the elongation of HS-85% increases from 14.0% to 15.9%. The mean size of dimples on the fracture surface of HS-85% sample shows a slight increase due to the abnormal grain growth, and the fracture mechanism is mainly dimple-induced transgranular fracture (Figs. 11(g) and (h)). Furthermore, the maximum texture density and its variation are small during spinning at 400 °C, so the effect of texture on mechanical properties may be weak.

3.3 Effect of room-temperature spinning on microstructure and mechanical properties of 7075 alloy tube

Figure 12 presents the EBSD results of the 7075 alloy tube after 85% thickness reduction at

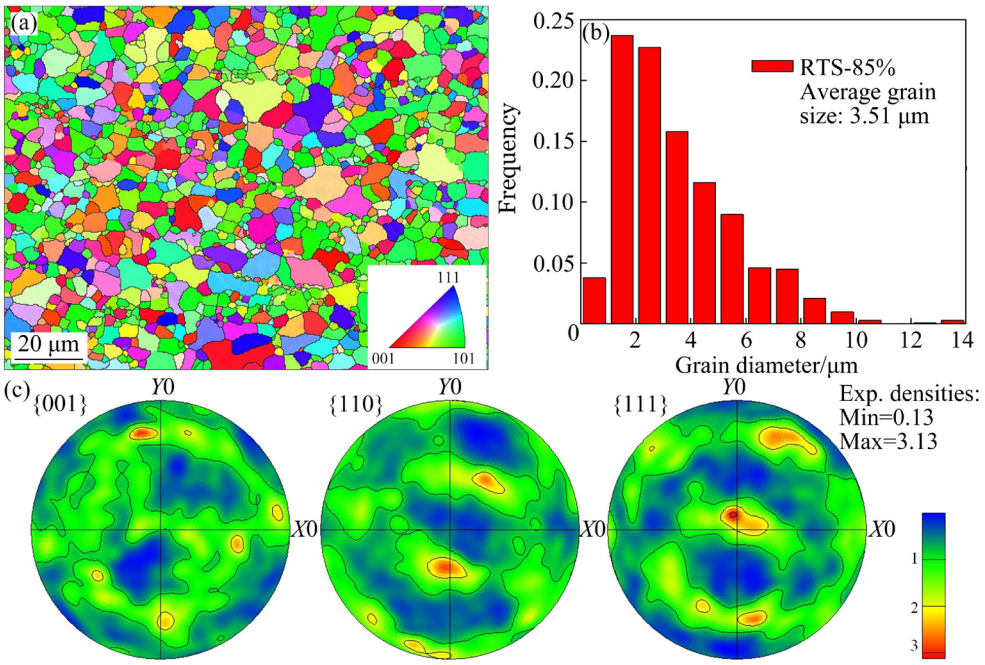

Fig. 12 EBSD results of 7075 alloy tube after 85% spinning deformation at room temperature: (a) Inverse pole figure map; (b) Grain diameter; (c) Pole intensity figure

room temperature. As shown in Figs. 12(a) and (b), after 85% thickness reduction at room temperature, the grains of RTS-85% sample are fragmented distinctly and the average grain size (d_{Ave}) is 3.51 μm due to the severe plastic deformation. And based on Fig. 12(b), the ratio of d_{max}/d_{Ave} is about 2.9. Compared with the sample of HS-85%, the d_{Ave} of the RTS-85% sample is slightly larger but the grain uniformity is higher. Moreover, as presented in Fig. 12(c), the RTS-85% sample shows a weak texture, and the maximum texture intensity is 3.13.

Figure 13 shows the TEM micrographs of the samples after 85% thickness reduction at room temperature and 400 °C, and the difference is distinct. As presented in Fig. 13(a), the dislocation density of the RTS-85% sample is very high, and a large number of dislocation pile-ups such as microbands (MBs) and cell blocks (CBs) are observed in the RTS-85% sample, which indicates the emergence of a strengthened work hardening. And the dislocation distribution is inhomogeneous after the room-temperature spinning due to the plastic strain localization. In addition, some elongated subgrains with relatively high intragranular dislocation density can be found in the microstructure, as shown in Fig. 13(b). This is attributed to the fact that the high stacking fault energy (SFE) in aluminum alloys and the large shear deformation can promote the dislocation alignment into LAGBs and thus the formation of the subgrains [20,21,41]. However, after spinning at 400 °C, the dislocation density of the HS-85% sample is significantly low and the dislocation tangles are rare, as shown in Figs. 13(c, d). And numerous sub-grains with defined grain boundaries and recrystallized grains can be found in the microstructure. This is attributed to the fact that the high deformation temperature can facilitate the slip and cross slip of dislocations and further stimulate the occurrence of DRV and DRX. The electron diffraction pattern in Fig. 13(d) shows that the recrystallized grain orientations are parallel to the [110] zone axis, showing its corresponding Al diffraction pattern.

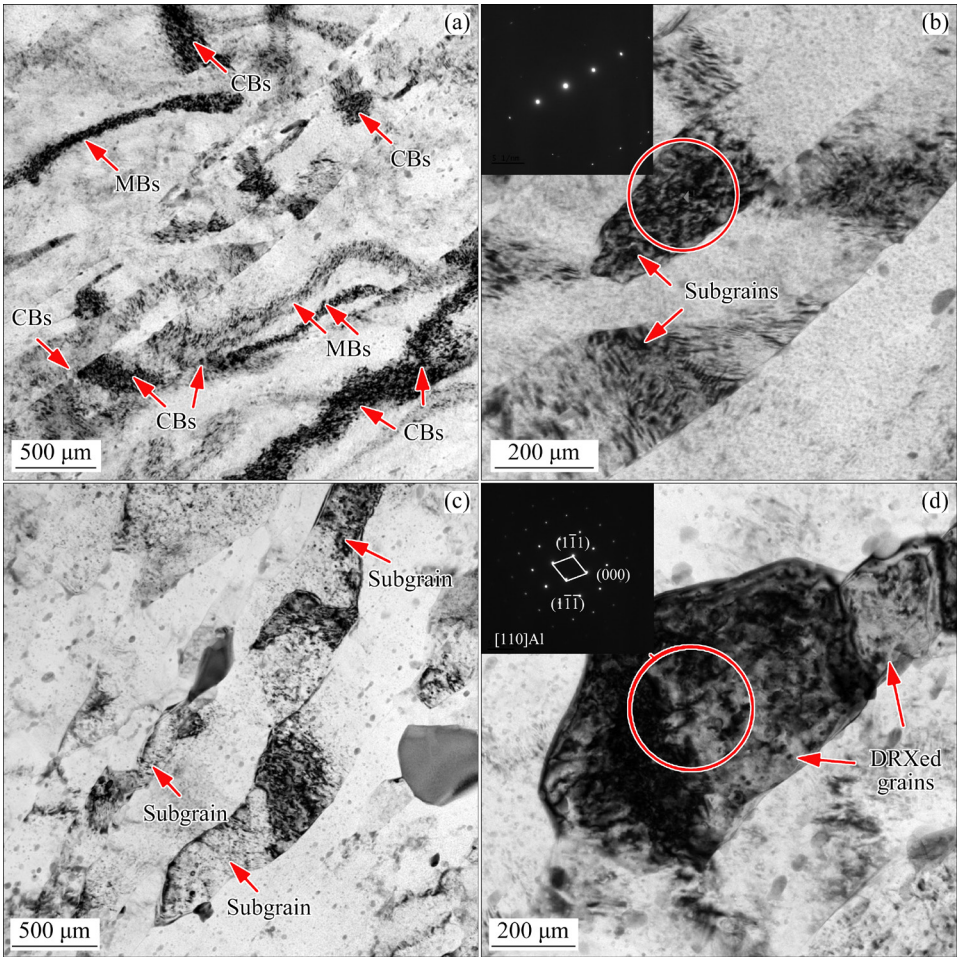

Fig. 13 TEM images of 7075 alloy tube after 85% thickness reduction at room temperature and 400 °C: (a, b) RTS-85%; (c, d) HS-85%

Figure 14 illustrates the engineering stress−strain curves of the 7075 alloy tube after 85% thickness reduction at RT and 400 °C. And the data for yield strength (YS), ultimate tensile strength (UTS) and elongation are summarized in Fig. 14. The YS, UTS and elongation of the 7075 alloy tube with 85% thickness reduction at 400 °C are 360.7 MPa, 458.7 MPa and 15.9%, respectively. And the YS, UTS and elongation of the RTS-85% sample after 85% thickness reduction at room temperature are 567.9 MPa, 613.5 MPa and 7.3%, respectively. The YS and UTS of RTS-85% sample are significantly higher than those of HS-85% sample, which are improved by 57.4% and 33.7%, respectively. However, the elongation of the RTS-85% sample is only 7.3%, which is lower than that of the HS-85%. On the microscopic scale, the work hardening behavior of crystalline materials is controlled by the dislocation multiplication, the dislocation tangle and the interaction between dislocations [13]. In addition, the high dislocation density could cause severe internal stress concentration, which results in the low elongation. Consequently, the higher YS and UTS and lower elongation of the RTS-85% sample are mainly due to the stronger work hardening (Fig. 13(a)). The fracture morphologies of the RTS-85% and HS-85% are presented in Fig. 15. Compared with that of the HS-85% sample, the dimples of the RTS-85% sample are shallower, and the cleavage facets (marked by red arrows) and the smooth regions (marked with red square frames) can be found on the fracture surface (Figs. 15(a, b)), which indicates the low ductility, and the brittle fracture is the main fracture mechanism.

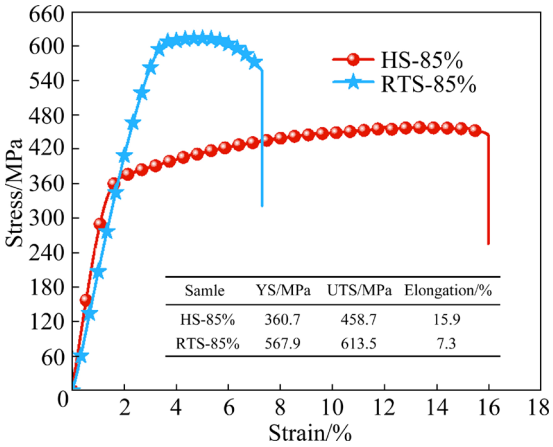

Fig. 14 Engineering stress−strain curves at RT and 400 °C after 85% thickness reduction

In addition, the obvious difference of the mechanical properties between RTS-85% and HS-85% will be further explained below. 7075 alloy belongs to a typical high strength aluminum alloy of 7000 series, which is difficult to be formed at room temperature due to the low metal liquidity and high strength [42]. Furthermore, the RTS-85% sample underwent 85% thickness reduction with two passes at room temperature, indicating a large single-pass spinning deformation, resulting in the more difficult deformation. Therefore, during room-temperature spinning, the low formability of the 7075 alloy and large single-pass spinning deformation not only cause a large number of dislocation multiplication and entanglement to produce macroscopic plastic deformation, but also result in a uneven internal deformation of the material due to the strain localization. Ultimately, this gives rise to the high dislocation density and

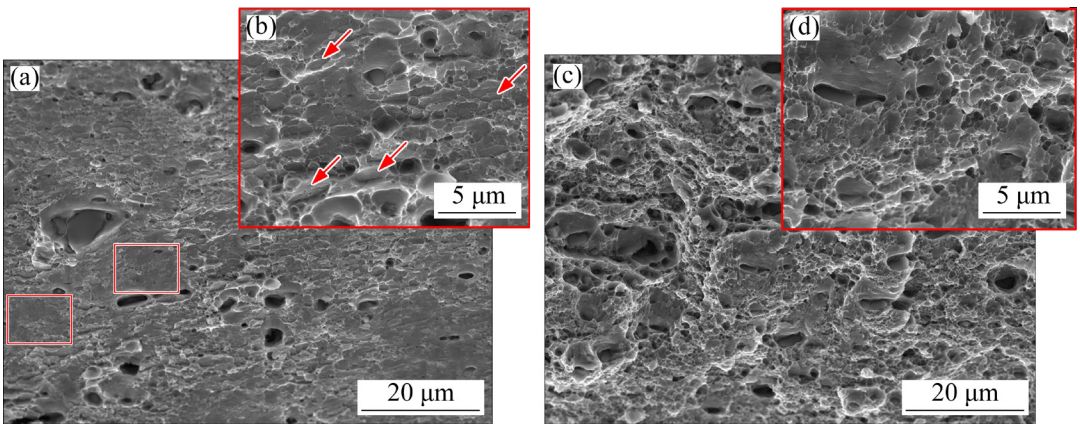

Fig. 15 SEM fracture surfaces of 7075 alloy tubes after 85% thickness reductions at room temperature (a, b) and at 400 °C (c, d)

the inhomogeneous distribution of dislocations in the microstructure of the RTS-85% sample (see Fig. 13(a)), which brings about a significant working hardening and stress concentration. This can be verified by the emergence of the shallow dimples, the cleavage facets and the smooth regions resulting from the severe stress concentration on the tensile fracture in Figs. 15(a) and (b) during tensile deformation. However, during spinning at 400 °C, the high temperature can improve the plasticity of materials and increase the fluidity of the 7075 alloy. And LU et al [43] illustrated that under uniaxial tensile tests at 400 °C, the maximum flow stresses of 7075-T6 aluminum alloy at strain rates of 0.1 and 1 s^{-1} are about 70 and 90 MPa, respectively. This indicates that the deformation resistance is very low and the dislocation movement becomes easy during spinning at 400 °C. Furthermore, during the three-pass spinning process, the spinning deformation per pass of the HS-85% sample is small. Therefore, the high deformation temperature and small single-pass spinning deformation cause more uniform deformation and less dislocation pile-up. And during spinning at 400 °C, the occurrence of dynamic recovery (DRV) and dynamic recrystallization (DRX) would further reduce the dislocation density through the formation of subgrains and recrystallized grains, as shown in Fig. 6(d), Fig. 8(d) and Figs. 13(c, d). Hence, the working hardening of the HS-85% sample is weaker distinctly than that of the RTS-85% sample, and there are more dimples on the fracture surface (Figs. 15(c) and (d)) due to the lower stress concentration. As a result, the above reasons result in the significant difference in mechanical properties between HS-85% and RTS-85% samples.

4 Conclusions

(1) After spinning, the grains are refined distinctly, and in the HS-60% and HS-70% samples, the deformed structure is dominant, while the recrystallized structure is dominant in the microstructure of HS-85% sample. Additionally, a bimodal grain structure with a weak Cube texture is obtained in the HS-85% sample due to the emergence of dynamic recrystallization (DRX) and abnormal grain growth.

(2) As the thickness reduction increases from 0% to 70% at 400 °C, the increase of the UTS and YS and the decrease of elongation are due to the combined effect of the grain refinement and work hardening, and the maximum UTS (468.8 MPa) and YS (365.0 MPa) and the minimum elongation (14.0%) are obtained during spinning at 400 °C.

(3) With the increase of thickness reduction from 70% to 85% at 400 °C, the decrease of the UTS and YS is mainly attributed to the reduction of dislocation density, and the increase of elongation is mainly due to the formation of bimodal grains and the weakening of work hardening.

(4) Compared with that of the HS-85% sample, the UTS and YS of RTS-85% sample are 613.5 and 567.9 MPa, respectively, which are improved by 33.7% and 57.4% due to the stronger work hardening, while the elongation is only 7.3%.

Acknowledgments

This work was supported by the National Natural Science Foundation of China (Nos. 51805358, 51775366), Key Research and Development Program of Jinzhong, China (No. Y201023), and College Students' Innovative Entrepreneurial Training Plan Program, China (No. 202010112011), and Shanxi Province Key Research and Development Project, China (No. 202102150401003).

References

[1] ZHAN Mei, YANG He, GUO Jing, WANG Xian-xian. Review on hot spinning for difficult-to-deform lightweight metals [J]. Transactions of Nonferrous Metals Society of China, 2015, 25(6): 1732−1743.

[2] GAO P F, LI M, ZHAN M, XING L, MA F, FU M W. Circumferential twist in flow forming of tubular parts: Characterization, understanding and control [J]. Journal of Manufacturing Processes, 2021, 65: 144−152.

[3] GUNAY E, FENERCIOGLU T O, YALCINKAYA T. Numerical analysis of thermo-mechanical behavior in flow forming [J]. Procedia Structural Integrity, 2022, 35: 42−50.

[4] VRIENS B C, HAGHSHENAS M, KLASSEN R J. Investigation of the effect of roller inclination angle on the forming forces during a splined mandrel flow forming operation [J]. Journal of Manufacturing Processes, 2015, 19: 183−186.

[5] SRIVASTWA A K, SINGH P K, KUMAR S. Experimental investigation of flow forming forces in Al7075 and Al2014—A comparative study [J]. Materials Today: Proceedings, 2021, 47: 2715−2719.

[6] ZENG X, FAN X G, LI H W, ZHAN M, ZHANG H R, WU K Q, REN T W, LI S H. Die filling mechanism in flow forming of thin-walled tubular parts with cross inner ribs [J].

Journal of Manufacturing Processes, 2020, 58: 832−844.

[7] LIU Jian, CHENG Yuan-sheng, CHAN S W N, SUNG D. Microstructure and mechanical properties of 7075 aluminum alloy during complex thixoextrusion [J]. Transactions of Nonferrous Metals Society of China, 2020, 30(12): 3173−3182.

[8] ZHOU Bing, LU Shuai, XU Kai-le, XU Chun, WANG Zhan-yong, WANG Bin-jun. Hot cracking tendency test and simulation of 7075 semi-solid aluminium alloy [J]. Transactions of Nonferrous Metals Society of China, 2020, 30(2): 318−332.

[9] BAEK M S, EUH K, LEE K A. Microstructure, tensile and fatigue properties of high strength Al 7075 alloy manufactured via twin-roll strip casting [J]. Journal of Materials Research and Technology, 2020, 9: 9941−9950.

[10] ZHANG R Y, WANG E L, ZHAO G Y, TU S J, GUO Z H. Effects of process parameters on elongation during hot power backward spinning for 7075 cast aluminium alloy tube [J]. Advanced Materials Research, 2013, 753/754/755: 183−186.

[11] ZHANG R Y, TU S J, ZHAO G Y, WANG J, GUO Z H. Evolution regularity of temperature filed in hot power backward spinning for 7075 cast aluminium alloy tube [J]. Advanced Materials Research, 2013, 774/775/776, 1170−1173.

[12] MOLLADAVOUDI H R, DJAVANROODI F. Experimental study of thickness reduction effects on mechanical properties and spinning accuracy of aluminum 7075-O during flow forming [J]. International Journal of Advanced Manufacturing Technology, 2011, 52: 949−957.

[13] LEI Z N, GAO P F, WANG X X, ZHAN M, LI H W. Analysis of anisotropy mechanism in the mechanical property of titanium alloy tube formed through hot flow forming [J]. Journal of Materials Science and Technology, 2021, 86(27): 77−90.

[14] YU C, SUN P, KAO P, CHANG C. Evolution of microstructure during annealing of a severely deformed aluminum [J]. Materials Science and Engineering A, 2004, 366: 310−317.

[15] JIANG J F, LIU Y Z, XIAO G F, WANG Y, JU Y G. Effect of pass reduction on microstructure, mechanical properties and texture of hot-rolled 7075 alloy [J]. Materials Characterization, 2019, 147: 324−339.

[16] XIAO H, LU Z, ZHANG K F, JIANG S S, SHI C C. Achieving outstanding combination of strength and ductility of the Al−Mg−Li alloy by cold rolling combined with electropulsing assisted treatment [J]. Materials & Design, 2020, 186: 108279.

[17] HUA L, HU X, HAN X H. Microstructure evolution of annealed 7075 aluminum alloy and its influence on room-temperature plasticity [J]. Materials & Design, 2020, 196: 109192.

[18] JIANG Ju-fu, WANG Ying, LIU Ying-ze, XIAO Guan-fei, LI Hua. Microstructure and mechanical properties of 7005 aluminum alloy processed by one-pass equal channel reciprocating extrusion [J]. Transactions of Nonferrous Metals Society of China, 2021, 31(3): 609−625.

[19] SIDOR J, PETROV R H, KESTENS L A I. Deformation, recrystallization and plastic anisotropy of asymmetrically rolled aluminum sheets [J]. Materials Science and Engineering A, 2010, 528: 413−424.

[20] EL-DANAF E A, SOLIMAN M S, ALMAJD A A. EBSD investigation of the microstructure and microtexture evolution of 1050 aluminum cross deformed from ECAP to plane strain compression [J]. Journal of Materials Science, 2011, 46(10): 3291−3308.

[21] ZHANG Y B, MISHIN O V. Stored energy and recrystallized microstructures in nickel processed by accumulative roll bonding to different strains [J]. Materials Characterization, 2017, 129: 323−328.

[22] MISHIN O, ZHANG Y, GODFREY A. The influence of multiscale heterogeneity on recrystallization in nickel processed by accumulative roll bonding [J]. Journal of Materials Science, 2017, 52: 2730−2745.

[23] SUN Z C, ZHENG L S, YANG H. Softening mechanism and microstructure evolution of as-extruded 7075 aluminum alloy during hot deformation [J]. Materials Characterization, 2014, 90: 71−80.

[24] LI Y H, JIANG Y Q, XU Q, MA A B, JIANG J H, LIU H, YUAN Y C, QIU C. Achieving single-pass high-reduction rolling and enhanced mechanical properties of AZ91 alloy by RD-ECAP pre-processing [J]. Materials Science and Engineering A, 2021, 804: 140717.

[25] HOSSEINY N, SHABAN A, TOROGHINEJAD M R. Effect of bimodal microstructure on texture evolution and mechanical properties of 1050 Al alloy processed through severe plastic deformation and subsequent annealing [J]. Materials Science and Engineering A, 2021, 820: 141580.

[26] LV Y T, DING Y , CUI H Z, LIU G H, WANG B H, CAO L M, LI L, QIN Z B, LU W J. Investigation of microscopic residual stress and its effects on stress corrosion behavior of NiAl bronze alloy using in situ neutron diffraction/EBSD/ tensile corrosion experiment [J]. Materials Characterization, 2020, 164: 110351.

[27] ZHANG C C, WEI H L, LIU T T, JIANG L Y, YANG T, LIAO W H. Influences of residual stress and micro-deformation on microstructures and mechanical properties for Ti−6.5Al−3.5Mo−1.5Zr−0.3Si alloy produced by laser powder bed fusion [J]. Journal of Materials Science and Technology, 2021, 75: 174−183.

[28] WRIGHT S I, NOWELL M M, FIELD D P. A review of strain analysis using electron backscatter diffraction [J]. Microscopy and Microanalysis, 2011, 17(3): 316−329.

[29] YAN C K, FENG A H, QU S J, CAO G J, SUN J L, SHEN J, CHEN D L. Dynamic recrystallization of titanium: Effect of pre-activated twinning at cryogenic temperature [J]. Acta Materialia, 2018, 154: 311−324.

[30] GUBICZA J, CHINH N Q, CSANADI T, LANGDON T, UNGÁR T. Microstructure and strength of severely deformed fcc metals [J]. Materials Science and Engineering A, 2007, 462: 86−90.

[31] HOWEYZE M, ARABI H, EIVANI A R, JAFARIAN H R. Strengthening of AA5052 aluminum alloy by equal channel angular pressing followed by softening at room temperature [J]. Materials Science and Engineering A, 2018, 720: 160−168.

[32] NAJAFI S, EIVANI A R, SAMAEE M, JAFARIAN H R,

ZHOU J. A comprehensive investigation of the strengthening effects of dislocations, texture and low and high angle grain boundaries in ultrafine grained AA6063 aluminum alloy [J]. Materials Characterization, 2018, 136: 60−68.

[33] TERHUNE S, SWISHER D, OH-ISH K I, HORITA Z, LANGDON T, MCNELLEY T. An investigation of microstructure and grain-boundary evolution during ECA pressing of pure aluminum [J]. Metallurgical and Materials Transactions A, 2002, 33: 2173−2184.

[34] DALLA T F, LAPOVOK R, SANDLIN J, THOMSON P, DAVIES C, PERELOMA E. Microstructures and properties of copper processed by equal channel angular extrusion for 1-16 passes [J]. Acta Materialia, 2004, 52(16): 4819−4832.

[35] BAGHDADI A H, SAJURI Z, OMAR M Z, RAJABI A. Friction stir welding parameters: Impact of abnormal grain growth during post-weld heat treatment on mechanical properties of Al−Mg−Si welded joints [J]. Metals, 2020, 10(12): 1607.

[36] MORI K I, ISHIGURO M, ISOMURA Y. Hot shear spinning of cast aluminum alloy parts [J]. Journal of Materials Processing Technology, 2009, 209(7): 3621−3627.

[37] HE J H, JIN L, WANG F H, DONG S, DONG J. Mechanical properties of Mg−8Gd−3Y−0.5Zr alloy with bimodal grain size distributions [J]. Journal of Magnesium and Alloys, 2017, 5: 423−429.

[38] GUO M, ZHU J, ZHANG Y, LI G, LIN T, ZHANG J, ZHUANG L. The formation of bimodal grain size distribution in Al−Mg−Si−Cu alloy and its effect on the formability [J]. Materials Characterization, 2017, 132: 248−259.

[39] ZHANG Z, VAJPAI S K, ORLOV D, AMEYAMA K. Improvement of mechanical properties in SUS304L steel through the control of bimodal microstructure characteristics [J]. Materials Science and Engineering A, 2014, 598: 106−113.

[40] KUBOTA K, MABUCHI M, HIGASHI K. Review processing and mechanical properties of fine-grained Mg alloys [J]. Journal of Materials Science, 1999, 34: 2255−2262.

[41] YANG Q Y, ZHOU Y L, TAN Y B, XIANG S, MA M, ZHAO F. Effects of microstructure, texture evolution and strengthening mechanisms on mechanical properties of 3003 aluminum alloy during cryogenic rolling [J]. Journal of Alloys and Compounds, 2021, 884: 161135.

[42] KAZEMI-NAVAEE A, JAMAATI R, AVAL H J. Asymmetric cold rolling of AA7075 alloy: The evolution of microstructure, crystallographic texture, and mechanical properties [J]. Materials Science and Engineering A, 2021, 824: 141801.

[43] LU J, SONG Y L, HUA L, ZHENG K L, DAI D G. Thermal deformation behavior and processing maps of 7075 aluminum alloy sheet based on isothermal uniaxial tensile tests [J]. Journal of Alloys and Compounds, 2018, 767: 856−869.

强力错距旋压 Al−Zn−Mg−Cu (7075)合金管材的显微组织与力学性能

郑凡林[1,2]，陈洪胜[1,2]，王文先[3]，高会良[1]，高永康[1]

1. 太原理工大学 机械与运载工程学院，太原 030024；
2. 山西省智能水下装备重点实验室，太原 030024；
3. 太原理工大学 材料科学与工程学院，太原 030024

摘　要：采用强力错距旋压技术在 400 ℃(HS)和室温(RTS)条件下制备 7075 铝合金管材，并对其成形过程中的显微组织演变和力学性能变化进行研究。结果表明：经过旋压变形后，7075 铝合金管材的晶粒明显细化，并且在 400 ℃下厚度减薄 60%和 70%(HS-60%和 HS-70%)的管材组织以变形组织为主，而厚度减薄 85% (HS-85%)的管材组织以再结晶组织为主。此外，HS-85%管材由于动态再结晶和异常晶粒长大的出现，形成了具有弱立方织构的双峰晶粒组织。随着 400 ℃下厚度减薄率从 0%增加到 85%，管材的屈服强度(YS)和极限抗拉强度(UTS)先增加后降低，而伸长率则先降低后增加。室温厚度减薄 85%(RTS-85%)的管材的 UTS 和 YS 分别为 613.5 和 567.9 MPa，与 HS-85%管材相比，分别提高了 33.7%和 57.4%，但其伸长率仅为 7.3%。

关键词：7075 铝合金；强力错距旋压；显微组织演变；双峰晶粒结构；异常晶粒长大；力学性能

(Edited by Xiang-qun LI)